Supplementary Material on the Methodology Part II
Final report on hydrodynamic modelling

Final report

Consultant: José C. Sánchez Garrido

Date: November 12, 2018

Division: Fisheries and Aquaculture Policy and Resources Division (FIA) /
Fisheries and Aquaculture Department

Programme/Project Number: GCP/INT/317 EC Year 9

Abstract

The hydrodynamic connectivity of 10 coastal habitat regions of sardine (*sardina pilchardus*) in the Alboran Sea (AS) was investigated. The results were derived from the outputs of a high-resolution circulation model of the AS that was run for one spawning season of sardine (November-March), used then as the basis of a Lagrangian Flow Network (LFN) analysis. Special attention was paid to the possible exchange of sardine early life stages (ELS; whose movements were represented by passive drifters in our model) between north and south habitat patches of sardine in the AS (boxes in LFN terminology). The numerical simulations indicate that self-recruitment is the most likely link of the LFN with an average value of 86.3‰ in boxes of north Alboran and 373.2‰ in boxes of south Alboran. The probability for north-south connectivity in the AS was of the order of 10-20‰. The transport of ELS from north-to-south resulted more likely than that from south-to-north. Overall, we estimated that as much as $\approx 0.5\%$ of the total spawning biomass of sardine in the AS can be transported in either direction. We also found that ELS from the Atlantic (boxes off Cadiz and Arcila) can be driven into boxes of the AS, especially from the southern Atlantic margin (off Arcila) and very rarely from Cadiz. The two Atlantic regions of the network were not connected with each other in any of the simulations. Additional runs showed that connectivity results are sensitive to the depth at which sardine ELS are transported by the currents. While the overall pattern of connectivity did not change dramatically with drifting depth, connectivity values increased substantially overall as sardine ELS were located at greater depth (at least up to 25 m depth). Connectivity values were also rather sensitive to the time at which ELS were released in each box of the LFN, suggesting that the mesoscale variability of the AS circulation (and perhaps also variability of the currents at shorter scales) can modulate substantially the exchange of sardine spawning material between the selected habitat patches. Although our analysis indicates that northern and southern habitat locations of sardine in the AS are not hydrodynamically isolated from each other, it remains to be determined if the flux of spawning material from one location to another is large enough, and the feeding conditions of the drifting ELS are good enough, to establish an actual biological link between sardine subpopulations north and south of the AS.

Contents

1. Introduction

The Alboran Sea is a highly dynamic region of the World Ocean. It features surface velocity currents of the order of 1-2 m/s, which are comparable to the swifter large-scale currents found in the ocean (e.g., the Gulf Stream or the Kuroshio Current). Such high velocities are the results of the strong density contrast (or pressure gradient) between the salty and cold water of the Mediterranean and the incoming fresher and somewhat warmer incoming water from the Atlantic. The potential energy storage in the front is also the source of short-scale instabilities and ocean eddies, whose associated vertical velocities fuel the high primary productivity of the basin, among other processes (Sánchez-Garrido et al. 2015). In turn, such high productivity sustains small pelagic fish and higher trophic levels, including a significant population (or populations) of sardine.

The objective of this report is to assess the hydrodynamic connectivity among different spawning regions of sardine in the basin. To do that, we apply a standard Lagrangian Flow Network (LFN) technique (Dubois et al., 2016; Padberg-Gehle and Schneide, 2017) analysis to the output of a high-resolution circulation model of the Gulf of Cadiz and the Alboran Sea. The model has been used for other scientific purposes in the recent past (Sánchez-Garrido et al. 2011, 2013, 2014; Sammartino et al. 2014, 2017), and has been used here to simulate the ocean currents (and other dynamic variables of the ocean) for the years 2003-2004. In particular, the analysis include the period Nov. 2003-March 2004, which is the main spawning season of sardine in the region.

The organization of this report is as follows. Section 2 provides a brief description of the model. Section 3 describes the configuration of the run to be analysed, whereas Section 4 shows the main circulation patterns of the simulation. Section 5 describes the set of lagrangian experiments conducted and the LFN methods employed. Section 6 analyses the mean connectivity patterns found as well as sensitivities to different parameters. Finally, Section includes a summary and discussion of the results.

2. Model description

The numerical experiments have been performed with the MIT general circulation model (MITgcm; Marshall et al. 1997a, b). The model configuration and its physical parameterizations were the same as described in Sanchez-Garrido et al. (2013), who developed an operational application of the Strait of Gibraltar and the AS based on the MITgcm source code.

The model domain is also similar to the domain used by Sanchez-Garrido et al. (2013). The grid horizontal resolution, in the range of 1500-2500 m in the AS, has been refined in the present study (Fig. S1; see supplementary material). The maximum resolution, $\Delta x = \Delta y = 400$ m, is reached within the Strait of Gibraltar. Such high resolution allows for an accurate representation of the irregular bottom topography and shoreline of the Strait, which in turn is required to capture its nonlinear and energetic dynamics (e.g. Sanchez-

Garrido et al. 2011). In the vertical coordinate, the model has 50 z-levels unevenly distributed in the water column (greater density of z-levels towards the surface; Fig. S1). The surface level has a thickness of 3 m. The grid has a total size of 680x96x50 points.

3. Experimental design

We have completed a hindcast simulation of the period November 2003-April 2004. This time of the year corresponds to the main spawning season of the European Sardine in the region (Coombs et al. 2006). The model forcing was derived from the following reanalysis products:

- Lateral forcing from Copernicus IBI (http://marine.copernicus.eu/) and includes daily fields of temperature, salinity and current velocity.

- Atmospheric forcing from the Med-Cordex database initiative (https://www.medcordex.eu/medcordex.php): near-surface wind speed, downward short wave and long wave radiation, air temperature, specific humidity and precipitation.

- Lateral forcing (barotropic component) from the storm surge operational model NIVMAR, from the Spanish institution of Puertos del Estado (http://opendap.puertos.es/thredds/catalog.html).

Tidal velocities were calculated according to the constituents derived by Sanchez-Garrido et al. (2013).

After preprocessing the described set of forcing, the model was run for the period mentioned earlier. The first 20 days of the simulation were not analyzed as this was the model spin-up period (the time required for the model to provide statistically stationary solutions). During the rest of the simulation, from November 20 to April 15, we stored monthly outputs of all dynamical variables. Additionally, we stored hourly outputs of sea surface height (SSH; for validation proposes, i.e. tides), daily sea surface temperature (SST) and velocity currents within the first 100 m of the water column. The later fields were stored every 30 minutes in order to compute particle trajectories with the highest possible accuracy.

4. Results of the hindcast simulation

4.1 Mesoscale circulation

The model SSH from December-to-March is shown in Fig. 1. The synoptic field displayed by this figure reveals the presence of a rather stable Eastern Alboran Gyre
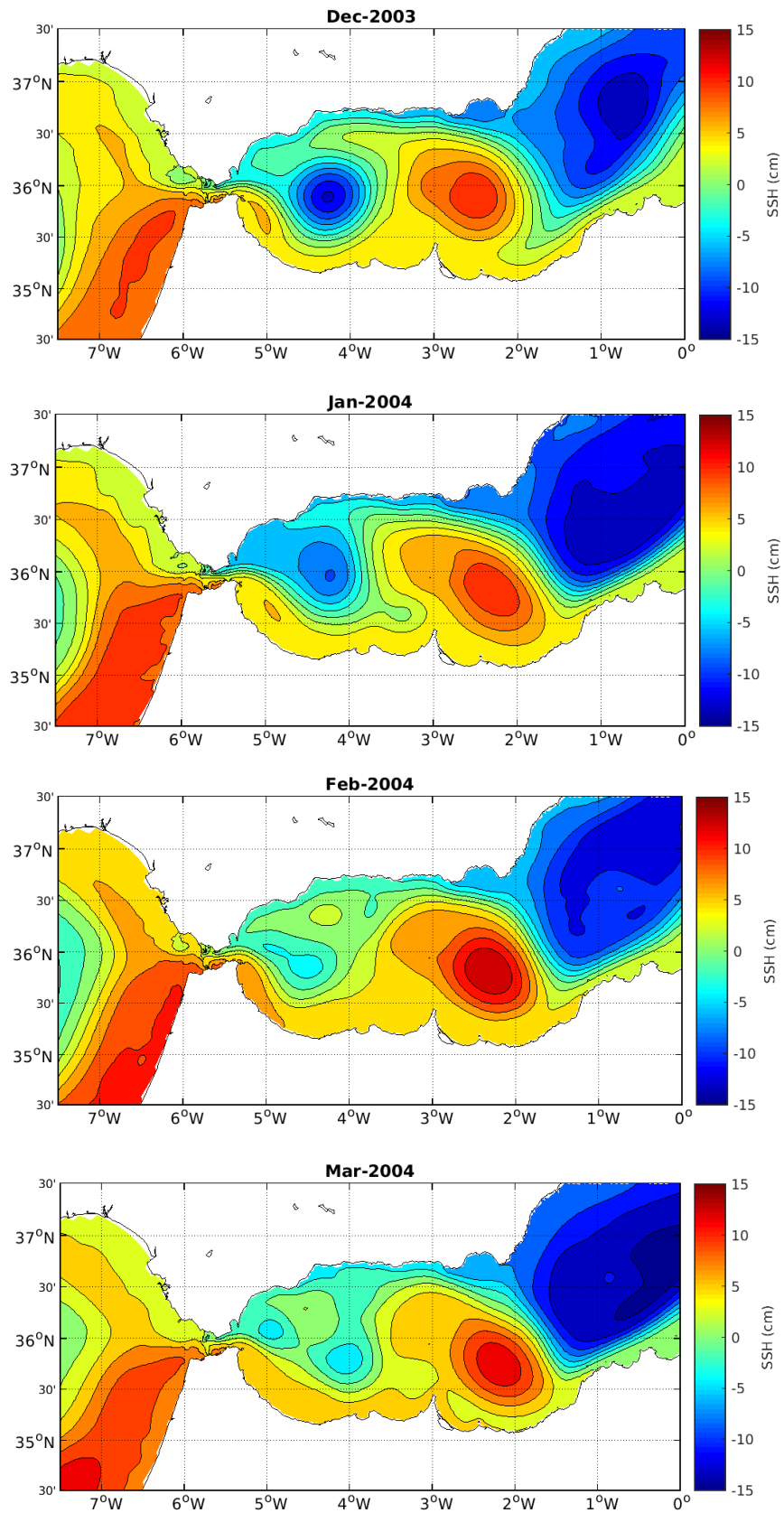

Fig. 1. Sea surface height as simulated by the circulation model. The fields shown

correspond to monthly means. From top to bottom: December 2003, January 2004, February 2004 and March 2004.

(EAG) and a weak Western Alboran Gyre (WAG). The latter structure appears as a small recirculation cell attached to the African coast that is fed by the jet of Atlantic Water entering through the Strait of Gibraltar. While this configuration changes little over time, one can observe a growing tendency of the WAG by the end of the simulation. This fact could be related to the concomitant weakening of the cyclonic gyre lying between the WAG and EAG. While this is not the most typical configuration reported in the AS, characterized by the presence of both the WAG and the EAG, the absence of one of the gyres is not rare. Surface currents and temperature (Fig. S2 and Fig. S3 respectively) confirm the above described picture.

4.2 Tidal and sub-inertial variability

A valuable feature of our simulation is the tidal forcing. Tides can be neglected in many parts of the Mediterranean, where they are generally weak. However, tides are very strong in some regions of our domain, particularly in the Strait of Gibraltar, and are also important over the shelf of the Gulf of Cadiz. Therefore, we believe that tides must play a noticeable role in determining larvae pathways from the Gulf of Cadiz to the AS. As such, tides were considered in our simulations.

Tidal charts corresponding to the main semidiurnal and diurnal tidal constituents are shown in Fig. 2. These charts have been derived from the model outputs, and are shown here for illustration and validation proposes. The larger surface tides correspond to the M_2 constituent. The associated amplitudes are as large as 1 m in the Gulf of Cadiz and 80 cm in the western part of the Strait of Gibraltar. Moving from east to west, M_2 amplitudes decay rapidly, reaching a value of only 30 cm at the eastern entrance of the Strait. The second most relevant constituent is S_2 (22-8 cm along the strait). Contrary to amplitudes, semidiurnal tidal phases exhibit a cross-strait structure with phases increasing from north to south. Diurnal amplitudes, of the order of few centimeters, are substantially weaker than those of the semidiurnal constituents. These tidal charts, particularly the semidiurnal ones, are similar to the charts published by García Lafuente et al. (1990).

While surface tides are illustrative, the potential impact of tidal currents on the drift of fish larvae becomes apparent by looking at tidal ellipses (Fig. S4). M_2 surface velocities can be as large as 1 m/s in the Strait of Gibraltar, which is the order of the mean velocity. As such, tidal currents can reverse the direction of the currents during part of the tidal cycle. This is well illustrated in Fig. 3, which shows a velocity time series at a selected point in the Strait of Gibraltar: zonal velocity (upper panel) becomes negative (surface current pointing to the Atlantic) over part of the referred cycle. One can also

distinguish sub-inertial variability in the velocity series (red line), very likely driven by synoptic atmospheric systems.
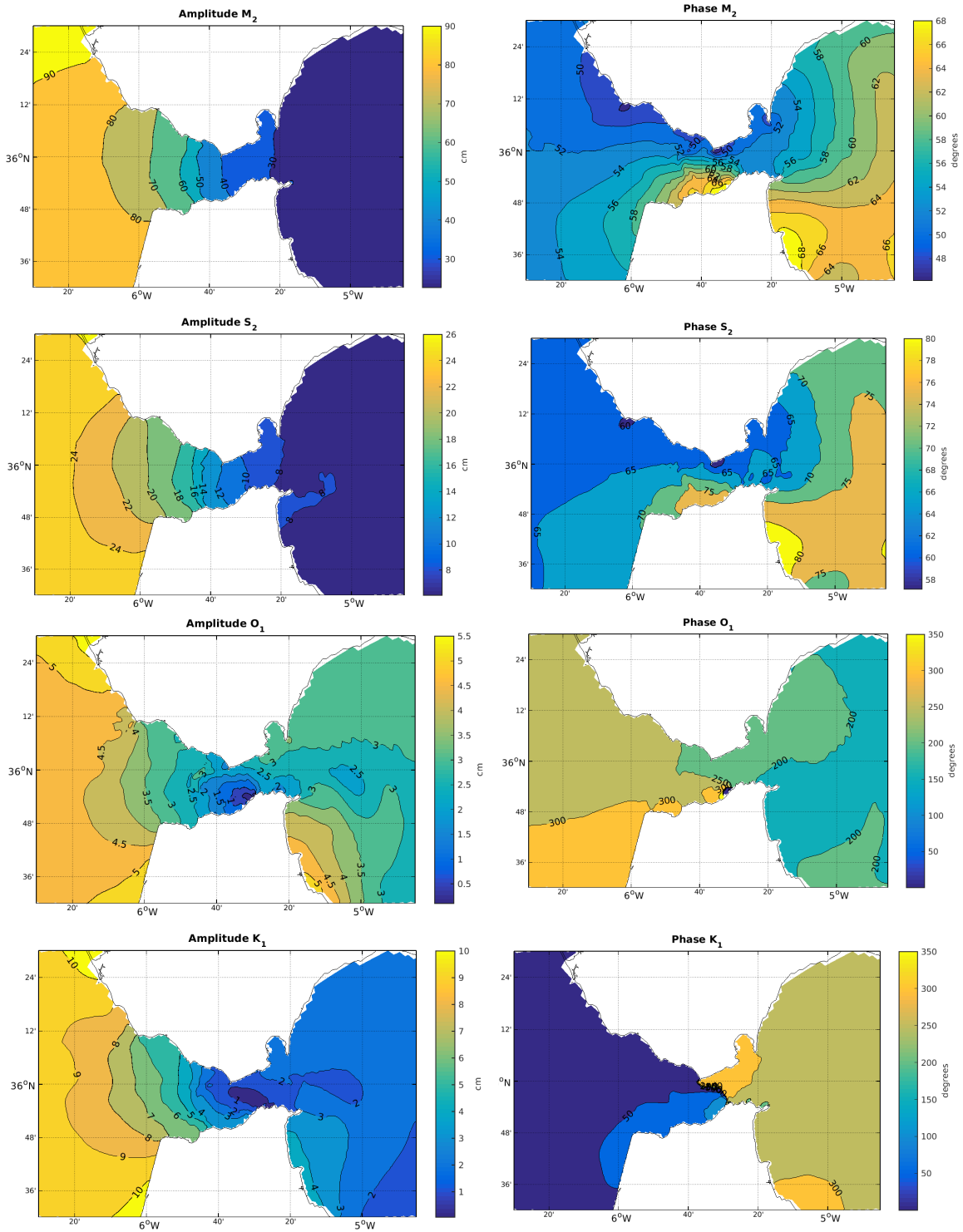

Fig. 2. Tidal charts of the mean semidirunal and diurnal tidal constituents at the Strait of Gibraltar. From top to bottom: M₂, S₂, O₁ and K₁. Tidal amplitudes are shown in the left column; tidal phases to the right.
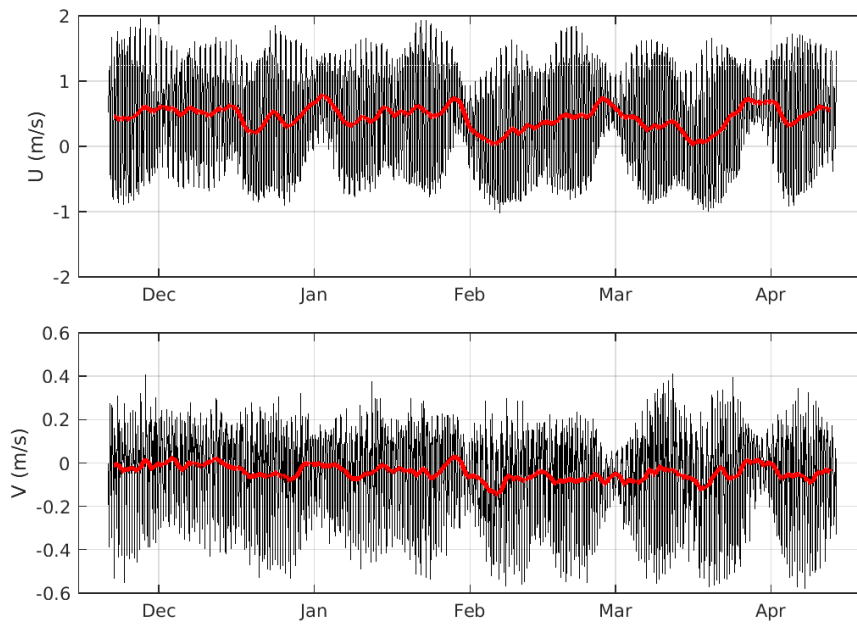
Fig. 3. Surface velocity time series at 5°45'W, 35° 56'N (Strait of Gibraltar). The zonal component (u) is shown in the upper panel, whereas the meridional component (v) is shown in the panel below. The red curve was obtained after applying a low-pass filter to the original simulated series (black line) and highlights sub-inertial variability present in the signal.

Lastly, it should be reminded that our model is three-dimensional (see, e.g., Fig. S5), and as long as we have stored velocity outputs at different depths, we will be able to simulate sardine larvae trajectories not only at the sea surface (sardine larvae are typically found at 0-25 m depth; García-García et al. 2016).

5. Particle tracking (lagrangian) experiments

5.1 Spawning regions and preliminary runs

Model velocity currents were used to simulate the drift of sardine larvae and investigate the hydrodynamic connectivity of different spawning areas of the AS. Larvae (or particles) were advected according to a lagrangian (or particle-tracking) algorithm implemented in our computational grid, similar to the one applied by Sammartino et al. (2017) [see also https://youtu.be/LVkDNDO9G2Q]. We considered 10 potential spawning regions distributed along the northern and southern coast of the AS (Fig. 4). Following the terminology of LFN techniques, these areas are referred to as boxes, or nodes, of the network. Boxes 1 and 6 lie to the west of the Strait of Gibraltar are therefore Atlantic areas; the rest of the boxes are located in the AS itself. The metric of connectivity is given by the ratio of particles arriving in one box after certain given time (representative of the sardine pelagic larval duration; hereinafter PLD) over the total

10

number of particles released in the initial box. This way, a probability matrix of the network can be built, P_{ij} $(i, j = 1, 2, ..., 10)$, where P_{ij} is the probability for one particle launched in box i to end up in box j. Except otherwise noted, the probability will be expressed in ‰.
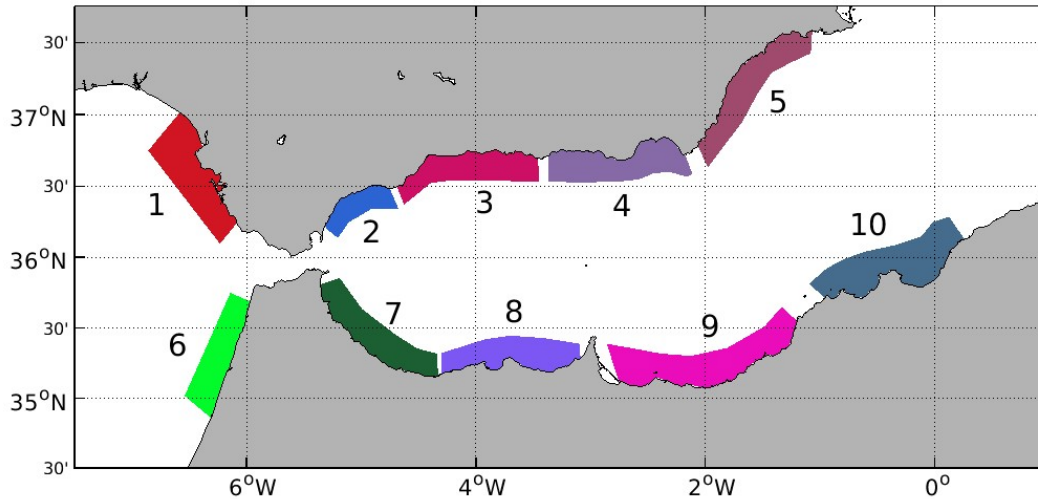

Fig. 4. Boxes of the Lagrangian Flow Network.

Prior to run the planned set of particle-tracking experiments (Section 5.2), a series of sensitivity runs were conducted to find the optimal time frequency at which model velocities had to be updated and utilized by the particle-tracking algorithm. Higher frequency implies more accurate trajectories, but also higher computational cost. Figure 5 shows different trajectories of the same particle in one of these sensitivity runs, with model velocity written every 15 min, 30 min, 60 min (hourly) and 1440 min (daily). The last two trajectories differ greatly from the one computed with Δt=15 min. (i.e., the benchmark), diverging from the latter at the entrance of the AS. In contrast, the trajectory with Δt=30 min. remains satisfactorily close to the reference pathway in the simulated period. The same behavior was found for other selected particles, from which we concluded that Δt=30 min. was the optimal writing periodicity to be used in the lagrangian algorithm.
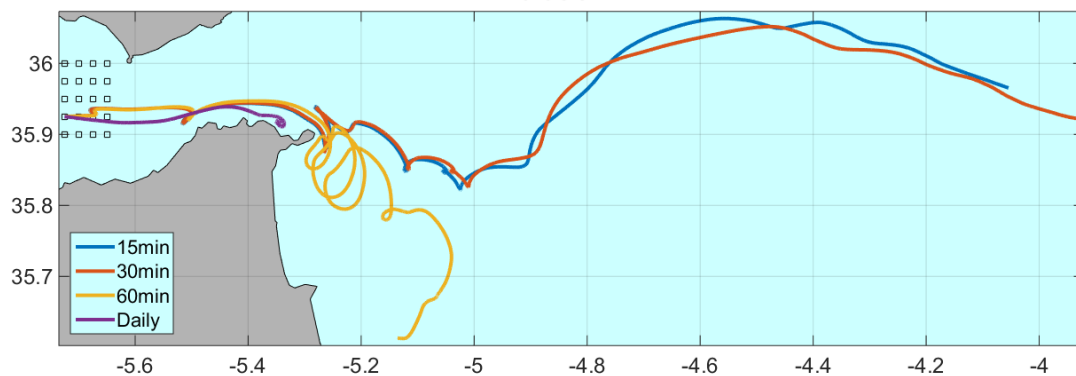

Fig. 5. Sensitivity runs of the particle tracking algorithm. Runs only differ in the frequency at which model velocity is updated and utilized by the lagrangian algorithm (the initial position and time release of the particle is the same for all the runs). The

optimal writing frequency was found to be 1/30 min^{-1}(trajectory in blue colour).

5.2 Experiments set

Around 1,000 particles were released in each box and tracked in space-time for 60 days. Particles were launched in the near-surface (z=1.5 m) and were assumed to remain at this depth along their drift. The same procedure was repeated 4 times over the whole simulated period, releasing particles every 40 days (table 1). Figure 6 shows all particle trajectories starting at Box #1 in the 4 mentioned experiments. The whole set of experiments implied the tracking of ~40,000 individual particles [(10 boxes) × (1.000 particles in each box) × (4 experiments)]. Because the initial position of the particles was assigned randomly, the incoming number of particles in every box is not identical in each experiment (some particles ended up inland prior to be advected by the currents).

With the above set of trajectories we evaluated the connectivity among the different boxes for PDL=50 days. Subsequently, this PLD value was set to 40 and 60 days to assess the sensitivity of the results against this parameter. Also, the different experiments allowed us to assess the sensitivity of the connectivity patterns to the time release of the particles (i.e., monthly variability of the patterns). Lastly, we evaluated the effect of larvae depth by conducting additional runs in which particles were advected at 12 m and 25 m depth (these two extra experiments covered the first simulated period only). Table 2 provides details of these runs.
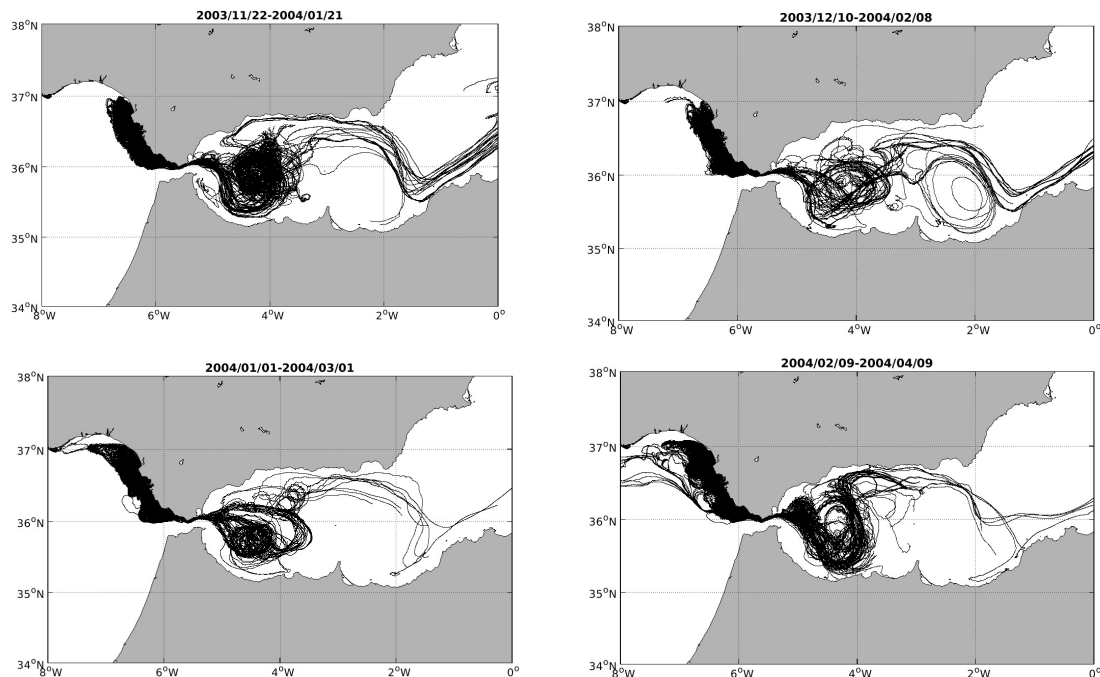

Fig. 6. Trajectory of the particles released in Box #1 at z=1.5 m. Top-left: period 22 Nov. 2003-21 Jan. 2004; top-right: 10 Dec. 2003-08 Feb. 2004; bottom-left: 01 Jan. 2004-01 Mar. 2004; bottom-right: 09 Feb. 2004-09 Apr.2004

Box \ Period	22 Nov. 2003-21 Jan. 2004	10 Dec. 2003-08 Feb. 2004	01 Jan. 2004-01 Mar. 2004	09 Feb. 2004-09 Apr.2004
B1	934	910	911	925
B2	1008	1011	1047	1026
B3	1150	1153	1156	1150
B4	1511	1398	1414	1377
B5	629	602	574	614
B6	811	923	950	895
B7	717	693	624	621
B8	1363	1370	1114	983
B9	894	941	927	935
B10	1037	1029	1037	1038

Table 1. Number of particles and periods of the baseline lagrangian experiments. All particles are advected at z=1.5 m depth.

Box \ Depth	z = 12 m	z = 25 m
B1	937	934
B2	1029	1031
B3	1087	1141
B4	1502	1525
B5	639	639
B6	969	940
B7	801	787
B8	1535	1599
B9	938	1826
B10	1008	1032

Table 2. Number of particles and selected depths for the sensitivity experiments. The time period of all runs is 22 Nov. 2003- 21 Jan. 2004.

6. Mean connectivity matrix

The mean connectivity matrix is shown in Table 3 (PLD=50 days; average over all experiments). The diagonal of the matrix (blue cells) correspond to the probability of self-recruitment, which are the greatest probability value for every row. Therefore, given a box, the most tightly connected box to it is the box itself. The probability of self-recruitment varies greatly among the different boxes, ranging from 27.7‰ in B5 to 567.5‰ in B6. Overall, self-recruitment in northern Alboran was less likely than in southern Alboran (86.3‰ versus 373.2‰). Cells in orange color are the most tightly connected box with the diagonal box (excluding self-recruitment). The overall west-to-east direction of the flow in our domain is reflected by the fact that orange cells are located to the right of the diagonal of the matrix. The exceptions to this rule are B5 and B10 which, of course, cannot send particles to boxes lying further east (B5 and B10 are the easternmost boxes of our domain).

Larval transport from the Atlantic to the Mediterranean boxes is much more likely to occur through the southern coastal margin. As much as 41.4‰ of the particles released

in B6 ended up in Mediterranean boxes (25‰ in B7 alone), whereas the same probability for particles launched in B1 was only 3.3‰. It is interesting to note that the Atlantic boxes do not receive particles from any other box of the network excluding themselves. Because of the strong inflow through the Strait of Gibraltar, the null transport of particles from the Mediterranean to the Atlantic was indeed expected, but the absence of connectivity between the two Atlantic boxes was less obvious.

Start\End	B1	B2	B3	B4	B5	B6	B7	B8	B9	B10
B1	555.16	0.00	0.00	0.27	0.00	0.00	0.27	0.54	0.82	1.36
B2	0.00	191.59	45.94	6.84	0.00	0.00	1.71	0.73	22.48	2.69
B3	0.00	5.21	43.83	10.63	0.22	0.00	0.00	0.00	1.08	3.69
B4	0.00	0.00	0.00	81.75	0.00	0.00	0.00	0.53	29.30	2.98
B5	0.00	0.00	0.00	11.16	27.70	0.00	0.00	0.00	6.20	2.48
B6	0.00	1.68	1.96	0.56	0.00	567.48	24.87	9.50	2.51	0.28
B7	0.00	1.51	9.04	9.42	0.00	0.00	434.27	69.68	22.98	15.07
B8	0.00	1.04	5.18	1.45	0.00	0.00	13.66	458.80	69.57	6.00
B9	0.00	0.81	0.54	0.54	0.00	0.00	0.00	1.89	307.82	22.45
B10	0.00	0.00	0.00	0.00	0.24	0.00	0.00	0.00	0.00	285.68

Table 3. Connectivity matrix for PLD=50 days and z=1.5 m (in ‰; average over all periods). Cells in blue colour correspond to self-recruitment values. Cells in orange colour indicate the maximum connectivity value for each box excluding self-recruitment.

Altogether, the connectivity matrix reflects that both north-to-south and south-to-north connectivity in the AS is possible. The clearest north-to-south pathway in the LFN is that connecting B4 with B9 (29.3‰), probably mediated by the eastern edge of the EAG (the so-called Almeria-Oran front). Regarding south-to-north connectivity, the strongest link is that between B7 and B4 (9.4‰). Considering all boxes in north (and south) Alboran as a whole, the probability for north-to-south connectivity (calculated as $\sum_{2\leq i\leq 5, j\geq 7} P_{i,j}/4$) was 18.6‰, whereas the probability for south-to-north connectivity ($\sum_{i\geq 7, 2\leq j\leq 5} P_{i,j}/4$) was estimated in 7.5‰. In terms of the sardine spawning biomass of sardine in the AS, currently distributed as ≈25% in the north and ≈75% in the south (personal communications with Dr. Manuel Hidalgo), the above calculations yield an expected 0.4% (=25% × 0.0186) of the total spawning material being carried from north-to-south, and 0.6% (=75% × 0.0075) from south-to-north.

7. Sensitivity analysis

7.1 PLD

The sensitivity of the connectivity matrix against PLD is examined here. Connectivity patterns are best visualized and compared in a color diagram of the matrix in question. The top-left panel of Fig. 7 is a color representation of Table 3 (in logarithm scale), with warm and cold colors indicating high and low probability. As discussed earlier, the probability of self-recruitment is the highest for every box, and so the diagonal of the

color diagram appears in yellow-to-red colors. The top-right and bottom panels represent the mean connectivity matrix for PLD=40 days and PLD=60 days respectively (the corresponding matrices can be found in the Supplementary Material); namely, 10 days shorter and longer than the information displayed in Table 3 (PLD=50). At first glance, the small differences among matrices indicate that the mean patterns discussed for PLD=50 days represents quite well the PLD range 40-60 days. Overall, the probability of north-to-south connectivity increases with PLD (Table 4; from 15.0‰ for PLD=40 days to 25.9‰ for PLD=60 days), whereas, curiously, the probability of south-to-north does the opposite, decreasing from 10.7‰ for PLD=40 days to 6.6‰ for PLD=60 days. The coefficient of variation (CV; or normalized standard deviation) of these two variables (occurrence of North-to-South and South-to-North connectivity) are of the same order (~0.25-0.30), suggesting that the hydrodynamic connectivity in both directions is equally sensitive to PLD.
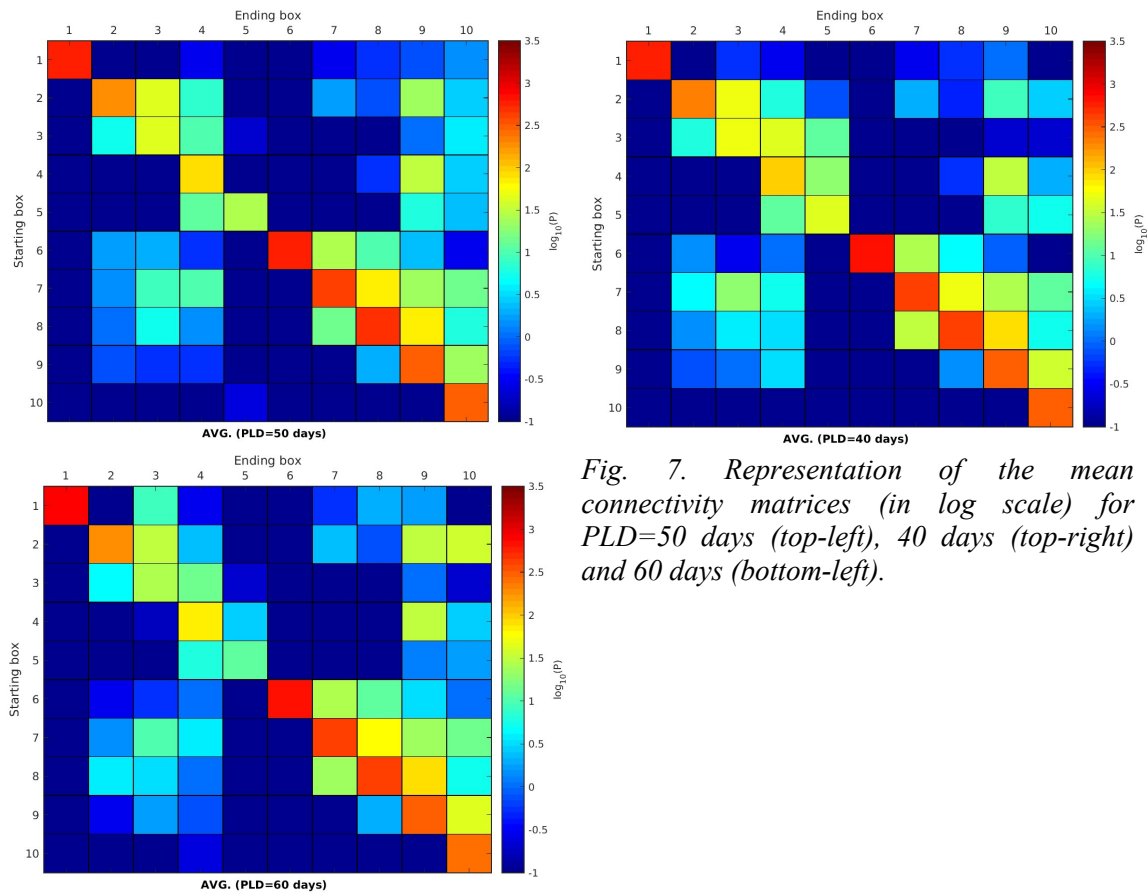

Fig. 7. Representation of the mean connectivity matrices (in log scale) for PLD=50 days (top-left), 40 days (top-right) and 60 days (bottom-left).

PLD \ Connectivity	North-to-South	South-to-North
40 days	15.0 ‰	10.7 ‰
50 days	18.6 ‰	7.5 ‰
60 days	25.9 ‰	6.6 ‰
Mean±Std	(19.8 ± 5.6) ‰	(8.3 ± 2.2) ‰
CV=Std/Mean	0.28	0.26

Table 4. Probability of north-to-south (boxes B1-B5 to B6-B10) and south-to-north (boxes B6-B10 to B1-B5) connection for different PLDs. The last two rows show the mean, the standard deviation and the coefficient of variation of the probability values.

7.2 Release time

Changes of the AS mesoscale circulation are expected to affect connectivity patterns substantially. The most notable mesoscale features of the AS are the WAG and the EAG, which can both either emerge or collapse in a time scale of few weeks (Sanchez-Garrido et al. 2015). In the present simulation, however, the circulation of the AS exhibits relatively weak mesoscale variability: the EAG is a stable feature and the WAG maintains a small size during the simulated period (showing a growing tendency though; Fig. 1). Despite this weak variability, the connectivity patterns of the 4 particle tracking experiments show noticeable differences (Fig. 8). For instance, Box #6 is only connected with Box #3 in the 2nd experiment, whereas all boxes except Box #1 receive particles from Box #6 in the 4th period. Another example of discrepancy between experiments is Box #4, which is only connected with itself in the 2nd run, but with other four different boxes (B2, B3, B9 and B10) in the 3rd run. Values of North-South connectivity in the AS (Table 5) indicate that the link from north-to-south is generally more likely than that from south-to-north, but also more variable in time (CV=1.2 vs. CV=0.27). These results suggest that the actual connectivity patterns of the AS could be subjected to significant mesoscale variability. Additional simulations would be necessary to obtain more reliable statistics.

Period \ Connectivity	North-to-South	South-to-North
1st (22 Nov. 2003- 21 Jan. 2004)	1.9 ‰	8.8 ‰
2nd (10 Dec. 2003-08 Feb. 2004)	2.5 ‰	5.6 ‰
3rd (01 Jan. 2004-01 Mar. 2004)	18.6 ‰	9.5 ‰
4th (09 Feb. 2004-09 Apr.2004)	51.5 ‰	5.8 ‰
Mean±Std	(18.6 ± 23.2) ‰	(7.4 ± 2.0) ‰
CV=Std/Mean	1.2	0.27

Table 5. Probability of north-to-south (boxes B1-B5 to B6-B10) and south-to-north (boxes B6-B10 to B1-B5) connectivity for all model runs. The last two rows show the mean, the standard deviation and the coefficient of variation of the probability values.
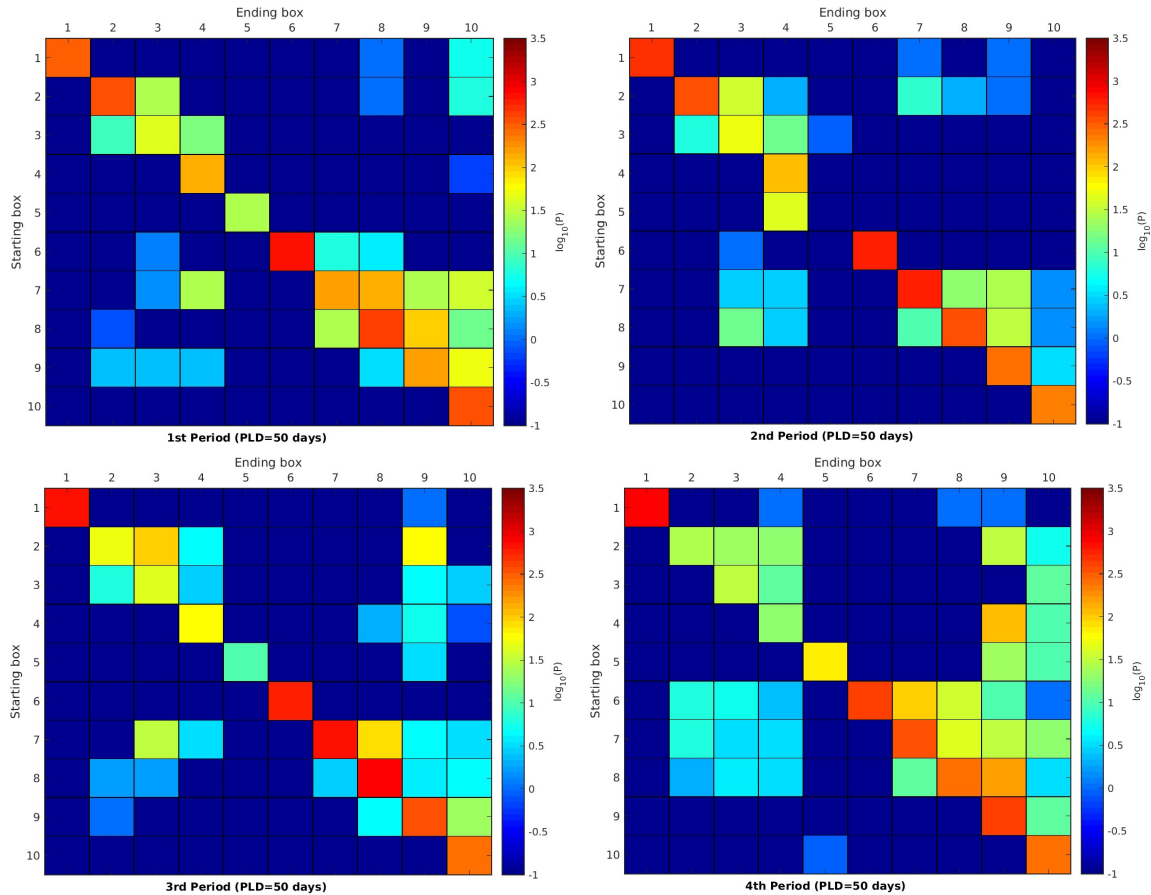
Fig. 8. Connectivity matrix for the four simulation periods (all for PLD=50 days).

7.3 Depth

The last sensitivity analysis concerns the depth at which sardine larvae were transported by the currents. The results discussed above correspond to larval drift at the near-surface (z=1.5 m). However, in field campaigns most of sardine larvae are found distributed in the first 20 m of the water column (García-García et al. 2016). We therefore examine the effect of larvae depth on the connectivity pattern.

Additional runs indicate that the connectivity of the different boxes become more likely as larvae are situated at greater depths (Fig. 9). The probability of North-to-South connectivity changes from ~1‰ at z=1.5 m to ~19‰ at z=25 m (Table 6), whereas the chances for south-to-north connection increase more moderately, from ~13‰ at z=1.5 m to ~20‰ at z=25 m. Hence, the north-to-south transport of particles appears as more sensitive to depth than the transport in the opposite direction. More thoughtful analyses would be needed to understand the processes involved for these outcomes, particularly for the enhanced probability of north-south connection with depth. A possible explanation for this later fact could be that velocity currents associated with the Atlantic jet, a hydrodynamic barrier preventing north-south connectivity, become weaker with depth, thereby making more feasible the transport of larvae across the AS at greater depths.
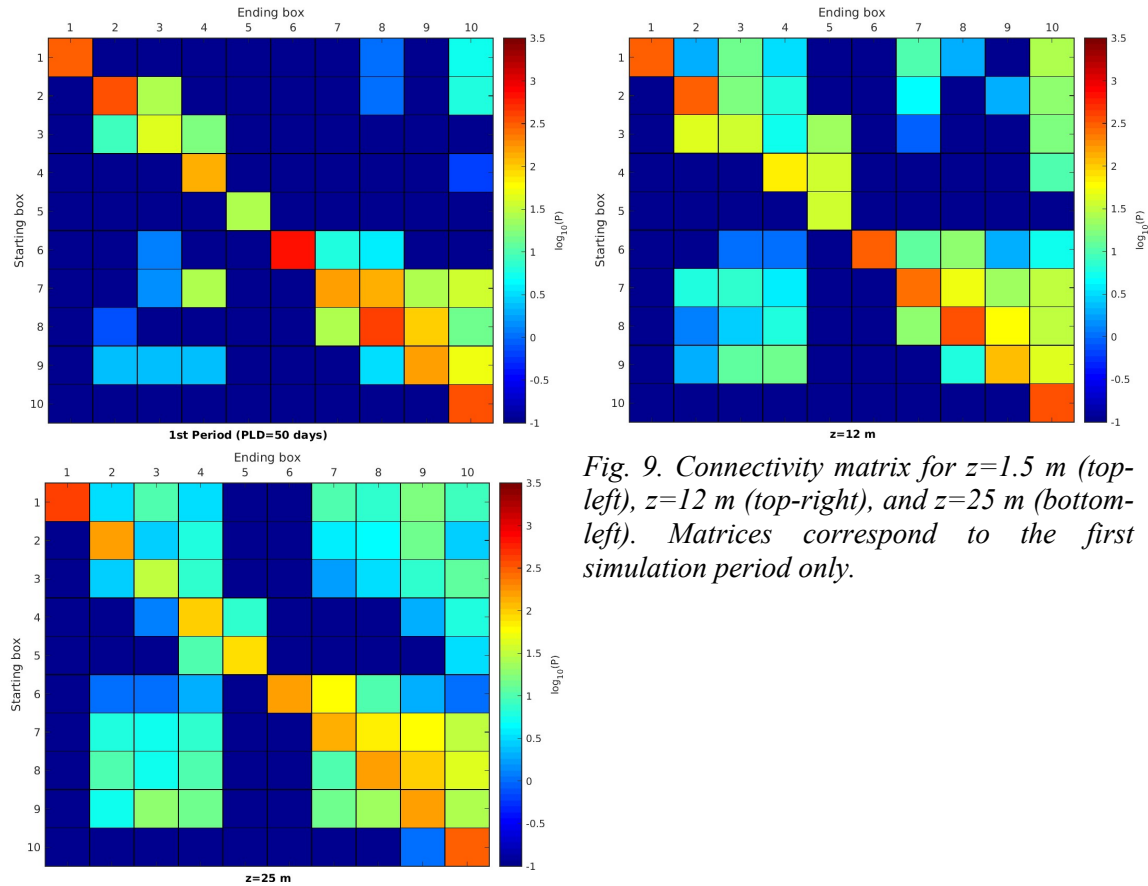
17

Fig. 9. Connectivity matrix for z=1.5 m (top-left), z=12 m (top-right), and z=25 m (bottom-left). Matrices correspond to the first simulation period only.

Depth \ Connectivity	North-to-South	South-to-North
z = 1.5 m	1.1 ‰	13.7 ‰
z = 12 m	7.7 ‰	22.6 ‰
z = 25 m	19.0 ‰	19.7 ‰
Mean±Std	(9.2 ± 9.1) ‰	(18.7 ± 4.5) ‰
CV=Std/Mean	0.99	0.24

Table 6. Probability of north-to-south (boxes B1-B5 to B6-B10) and south-to-north (boxes B6-B10 to B1-B5) connectivity for different depths. The last two rows show the mean, the standard deviation and the coefficient of variation of the probability values.

8. Summary and conclusions

On the basis of the output of a high-resolution circulation model of the AS, and applying a standard LFN analysis technique, we have studied the hydrodynamic connectivity of 10 selected spawning regions of sardine in the region. The results described herein correspond to a hindcast simulation of the period Nov. 2003-Mar. 2004, which covers the mean spawning season of sardine in these two years.

The probability for connection between north and south spawning areas (or boxes) was of the order of 10-20‰ (the transport from north-to-south being somewhat more likely; Table 3 and Fig. 7; top-left panel), suggesting that the interdependence, or mixture,

between sardine populations at both sides of the AS basin could occur. However, whether or not this interdependence is actually feasible will depend, among other biological factors, on both the number of eggs spawned in each region and the mortality rate of the drifting larvae, which are both uncertain quantities. We also found that there is a non-null input of particles form the Atlantic to the Mediterranean boxes, fundamentally through the southern margin of the Strait of Gibraltar and the AS (~40‰ in the south against ~3‰ in the north; Table 3). Therefore, we conclude that the connectivity between south and north sardine populations in the AS, as well as between Atlantic and Mediterranean populations, should not be ruled out.

Additional runs show that our results are sensitive to depth. While the patterns of connectivity do not change dramatically, it is true that the overall probability for connectivity between boxes increases substantially as larvae were located at greater depth (at least up to 25 m depth). More thoughtful research is needed to clarify the origin of this enhancement of probability but, whatever the physical processes involved are, this outcome suggests that our probability values for connectivity, calculated for larvae drifting in the near surface, could be somewhat underestimated.
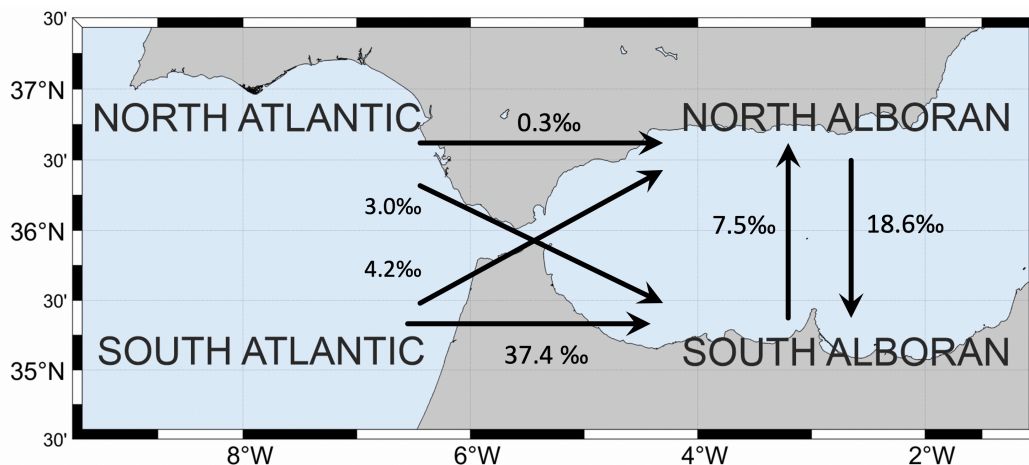
Fig. 10. Sketch of the mean connectivity pattern of the LFN.

Another variable that we found important is the time release of the particles. In this study statistics for connectivity were made based on four different lagrangian experiments, each of them starting at different months of the spawning season of sardine. The obtained connectivity values differed noticeably from one month to another, suggesting that the mesoscale variability of the flow (and perhaps also variability of shorter scale; e.g., tides), affects greatly the exchange of particles among boxes. It would be desirable to extend our simulations to additional years in order to obtain a broader variety of circulation scenarios of the AS. These scenarios should ideally include situations in which only one gyre (either the WAG or the EAG) or the two gyres are present (the scenario here would correspond to the first situation). This ample set of data would allow for the assessment of more robust patterns and metrics of the hydrodynamic connectivity between the selected coastal regions of the AS.

Acknowledgements

References

Coombs, S., Smyth, T., Conway, D., Halliday, N., Bernal, M., Stratoudakis, Y., & Alvarez, P., 2006. Spawning season and temperature relationships for sardine (Sardina pilchardus) in the eastern North Atlantic. Journal of the Marine Biological Association of the United Kingdom, 86(5), 1245-1252. doi:10.1017/S0025315406014251.

Dubois, M., Rossi, V., Ser-Giacomi, E., Arnaud-Haond, S., López, C., and Hernández-García, E. 2016. Linking basin-scale connectivity, oceanography and population dynamics for the conservation and management of marine ecosystems: Large-scale connectivity and management of marine ecosystems. Global Ecology and Biogeography, 25(5):503-515.

García-García, L. M., M. Ruiz-Villarreal, M. Bernal, 2016. A biophysical model for simulating early life stages of sardine in the Iberian Atlantic stock, Fisheries Research, 173, 3, 250-272.

García Lafuente, J., J.L. Almazán, F. Castillejo, A. Khribeche and A. Hakimi, 1990. Sea level in the Strait of Gibraltar: tides. International Hydrographic Review, LXVII.

Marshall, J., C. Hill, L. Perelman, and A. Adcroft, 1997. Hydrostatic, quasi-hydrostatic, and non-hydrostatic ocean modeling, J. Geophysical Res., 102(C3), 5733-5752.

Marshall, J., A. Adcroft, C. Hill, L. Perelman, and C. Heisey, 1997. A finite-volume, incompressible Navier Stokes model for studies of the ocean on parallel computers, J. Geophysical Res., 102(C3), 5753-5766.

Padberg-Gehle, K. and Schneide, C. (2017). Network-based study of Lagrangian transport and mixing. Nonlinear Processes in Geophysics, 24, 661-671.

Sammartino, S., J. García Lafuente, J.C. Sánchez Garrido, F.J. De los Santos, E. Álvarez Fanjul, C. Naranjo, M. Bruno, C. Calero, 2014. A numerical model analysis of the tidal flows in the Bay of Algeciras, Strait of Gibraltar. Continental Shelf Research, 72, 34-46.

Sammartino, S., J.C. Sánchez-Garrido, J. García Lafuente, M. García Sotillo, P. Rodríguez, 2017. Water renewal in semi-enclosed basins: a high resolution Lagrangian model approach with application to the Bay of Algeciras, Strait of Gibraltar. Limnol. Oceanogr. Methods. doi:10.1002/lom3.10231.

Sánchez-Garrido, J.C., J. García Lafuente; E. Álvarez Fanjul; M.G. Sotillo; F.J. de los Santos., 2013. What does cause the collapse of the western Alboran Gyre? Results of an operational ocean model. Progress in Oceanography. 116, pp. 142 - 153.

Sánchez-Garrido, J.C., G. Sannino; L. Liberti; J. García Lafuente; L. Pratt, 2011. Numerical modeling of three-dimensional stratified tidal flow over Camarinal Sill, Strait of Gibraltar. Journal of Geophysical Research: Oceans. 116 - C12, pp. n/a - n/a.

Sánchez-Garrido, J.C., C. Naranjo, D. Macías, J. García Lafuente, T. Oguz, 2015. Modeling the impact of tidal flows on the biological productivity of the Alboran Sea, 120, 7329-7345.

Supplementary material:
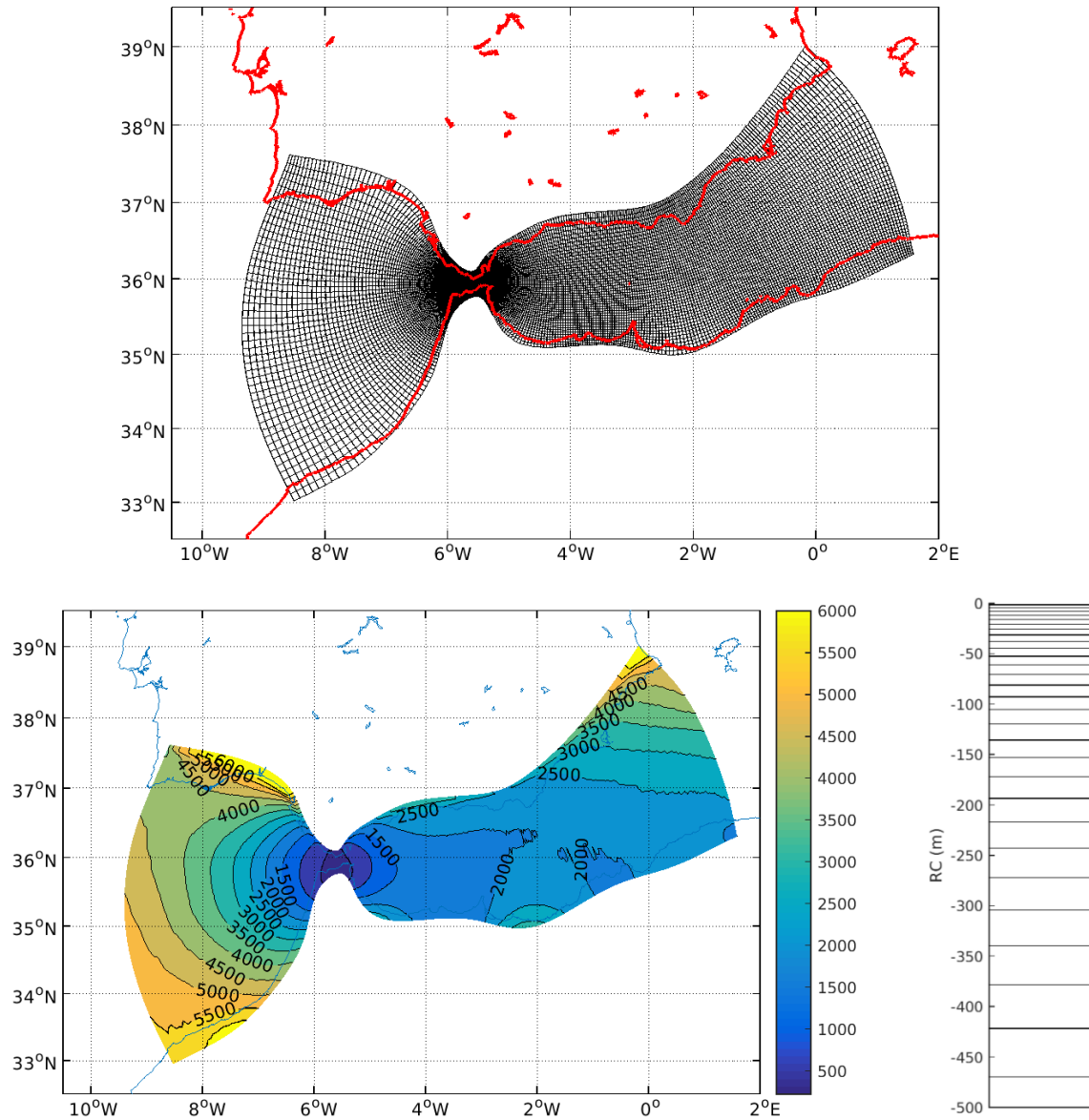
Fig. S1. Upper panel: computational grid used in the study. For the sake of clarity, only one of every four grid cell is shown. Bottom left: Horizonal grid resolution in meters. Bottom right: Vertical spatial discretization in the upper 500 m of the water columm.
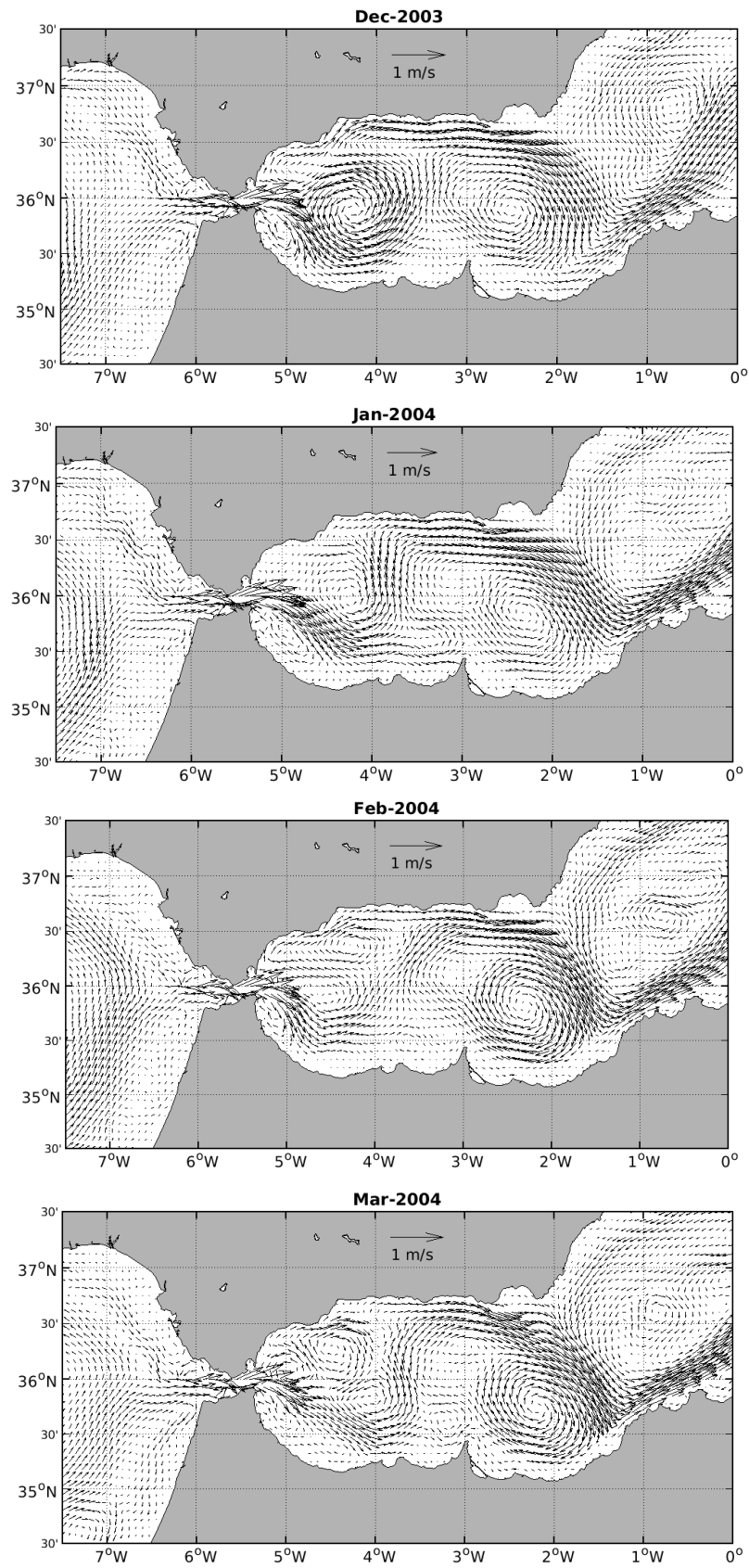
Fig. S2. Sea surface velocity as simulated by the circulation model. The fields shown correspond to monthly means. From top to bottom: December 2003, January 2004, February 2004 and March 2004.
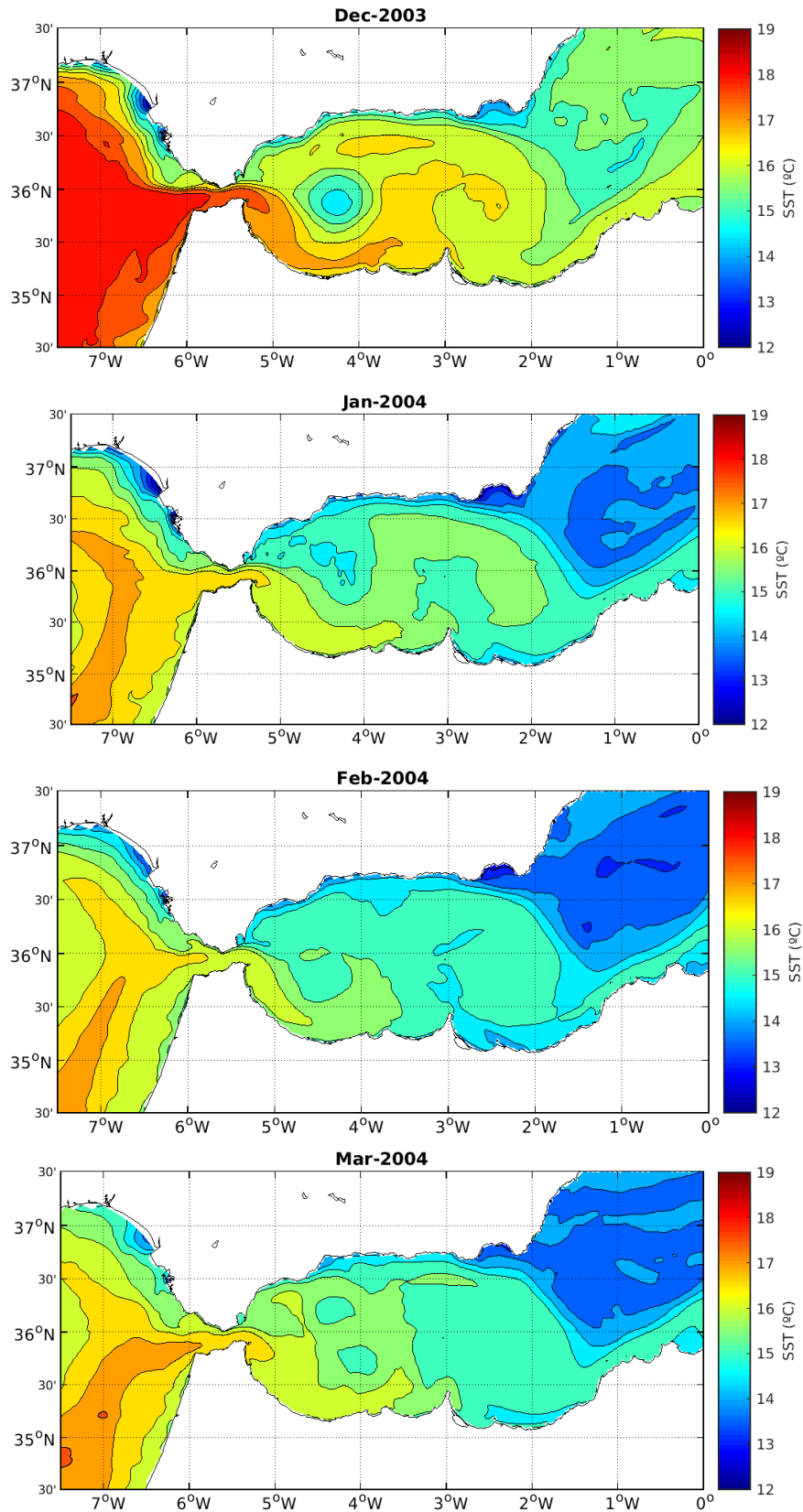
Fig. S3. Sea surface temperature as simulated by the circulation model. The fields shown correspond to monthly means. From top to bottom: December 2003, January 2004, February 2004 and March 2004.
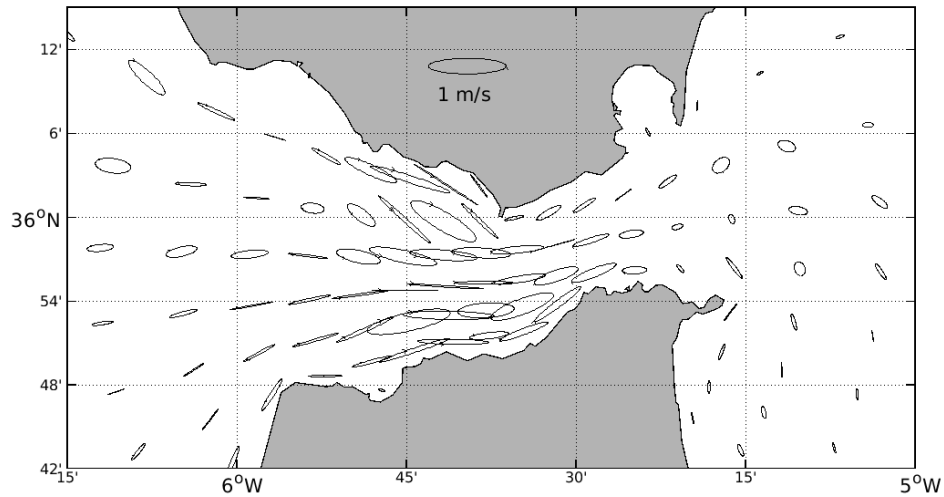
Fig. S4. M$_2$ surface current ellipses at the Strait of Gibraltar.
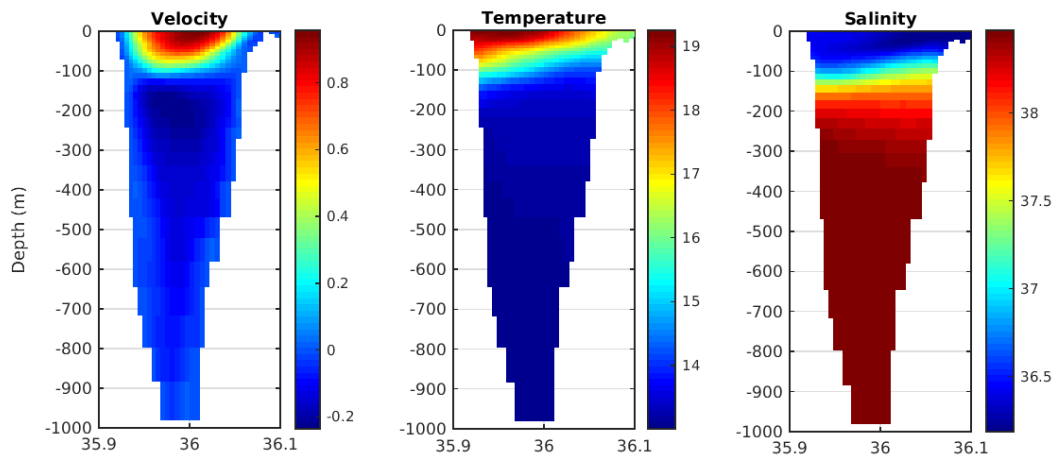
Fig. S5. Zonal velocity (left; m/s), temperature (centre; ℃) and salinity across the eastern mouth of the Strait of Gibraltar. The fields shown correspond to Dec. 2003 (monthly value).

Start\End	B1	B2	B3	B4	B5	B6	B7	B8	B9	B10
B1	555.16	0.00	0.00	0.27	0.00	0.00	0.27	0.54	0.82	1.36
B2	0.00	191.59	45.94	6.84	0.00	0.00	1.71	0.73	22.48	2.69
B3	0.00	5.21	43.83	10.63	0.22	0.00	0.00	0.00	1.08	3.69
B4	0.00	0.00	0.00	81.75	0.00	0.00	0.00	0.53	29.30	2.98
B5	0.00	0.00	0.00	11.16	27.70	0.00	0.00	0.00	6.20	2.48
B6	0.00	1.68	1.96	0.56	0.00	567.48	24.87	9.50	2.51	0.28
B7	0.00	1.51	9.04	9.42	0.00	0.00	434.27	69.68	22.98	15.07
B8	0.00	1.04	5.18	1.45	0.00	0.00	13.66	458.80	69.57	6.00
B9	0.00	0.81	0.54	0.54	0.00	0.00	0.00	1.89	307.82	22.45
B10	0.00	0.00	0.00	0.00	0.24	0.00	0.00	0.00	0.00	285.68

*Table S1. Connectivity matrix for PLD=50 days and z=1.5 m (in ‰; average over all periods). Cells in blue colour correspond to self-recruitment values. Cells in brown colour indicate the maximum connectivity value for each box, excluding self-recruitment.*

Start\End	B1	B2	B3	B4	B5	B6	B7	B8	B9	B10
B1	593.75	0.00	0.54	0.27	0.00	0.00	0.27	0.54	1.09	0.00
B2	0.00	234.60	50.83	6.60	0.73	0.00	1.96	0.49	8.80	2.69
B3	0.00	6.29	54.46	45.35	12.80	0.00	0.00	0.00	0.22	0.22
B4	0.00	0.00	0.00	95.96	20.00	0.00	0.00	0.53	30.35	2.11
B5	0.00	0.00	0.00	11.16	40.51	0.00	0.00	0.00	7.03	4.96
B6	0.00	1.40	0.28	1.12	0.00	723.67	28.50	4.75	0.84	0.00
B7	0.00	4.14	20.72	5.27	0.00	0.00	451.98	53.48	26.37	11.30
B8	0.00	1.45	3.73	3.52	0.00	0.00	31.26	445.55	80.75	5.18
B9	0.00	0.81	1.08	3.25	0.00	0.00	0.00	1.35	317.55	37.60
B10	0.00	0.00	0.00	0.00	0.00	0.00	0.00	0.00	0.00	291.72

Table S2. Connectivity matrix for PLD=40 days and z=1.5 m (in ‰; average over all periods). Cells in blue colour correspond to self-recruitment values. Cells in brown colour indicate the maximum connectivity value for each box, excluding self-recruitment.

Start\End	B1	B2	B3	B4	B5	B6	B7	B8	B9	B10
B1	736.68	0.00	8.97	0.27	0.00	0.00	0.54	1.90	1.63	0.00
B2	0.00	174.24	30.79	2.20	0.00	0.00	2.20	0.73	29.33	34.95
B3	0.00	4.77	26.47	13.89	0.22	0.00	0.00	0.00	1.08	0.22
B4	0.00	0.00	0.18	73.51	2.81	0.00	0.00	0.00	30.00	2.63
B5	0.00	0.00	0.00	5.79	12.82	0.00	0.00	0.00	1.24	1.65
B6	0.00	0.28	0.56	1.12	0.00	691.25	27.38	12.85	3.07	1.12
B7	0.00	1.51	10.55	3.77	0.00	0.00	429.00	58.76	24.48	15.07
B8	0.00	3.93	3.52	1.04	0.00	0.00	22.15	412.63	88.41	5.18
B9	0.00	0.27	1.62	0.81	0.00	0.00	0.00	2.16	319.18	44.09
B10	0.00	0.00	0.00	0.24	0.00	0.00	0.00	0.00	0.00	275.05

Table S3. Connectivity matrix for PLD=60 days and z=1.5 m (in ‰; average over all periods). Cells in blue colour correspond to self-recruitment values. Cells in brown colour indicate the maximum connectivity value for each box, excluding self-recruitment.

Start\End	B1	B2	B3	B4	B5	B6	B7	B8	B9	B10
B1	303.00	0.00	0.00	0.00	0.00	0.00	0.00	1.07	0.00	5.35
B2	0.00	337.30	26.79	0.00	0.00	0.00	0.00	0.99	0.00	5.95
B3	0.00	8.70	44.35	15.65	0.00	0.00	0.00	0.00	0.00	0.00
B4	0.00	0.00	0.00	136.33	0.00	0.00	0.00	0.00	0.00	0.66
B5	0.00	0.00	0.00	0.00	25.44	0.00	0.00	0.00	0.00	0.00
B6	0.00	0.00	1.23	0.00	0.00	684.34	6.17	3.70	0.00	0.00
B7	0.00	0.00	1.39	26.50	0.00	0.00	170.15	128.31	27.89	34.87
B8	0.00	0.73	0.00	0.00	0.00	0.00	27.88	413.79	99.78	13.94
B9	0.00	2.24	2.24	0.00	0.00	0.00	0.00	3.36	168.90	52.57
B10	0.00	0.00	0.00	0.00	0.00	0.00	0.00	0.00	0.00	368.37

Table S4. Connectivity matrix for PLD=50 days and z=1.5 m (in ‰; 1st period only). Cells in blue colour correspond to self-recruitment values. Cells in brown colour indicate the maximum connectivity value for each box, excluding self-recruitment.

Start\End	B1	B2	B3	B4	B5	B6	B7	B8	B9	B10
B1	509.89	0.00	0.00	0.00	0.00	0.00	1.10	0.00	1.10	0.00
B2	0.00	361.03	39.56	1.98	0.00	0.00	6.92	1.98	0.99	0.00
B3	0.00	6.07	50.30	13.01	0.87	0.00	0.00	0.00	0.00	0.00
B4	0.00	0.00	0.00	106.58	0.00	0.00	0.00	0.00	0.00	0.00
B5	0.00	0.00	0.00	44.85	0.00	0.00	0.00	0.00	0.00	0.00
B6	0.00	0.00	1.08	0.00	0.00	599.13	0.00	0.00	0.00	0.00
B7	0.00	0.00	2.89	2.89	0.00	0.00	575.76	20.20	27.42	1.44
B8	0.00	0.00	13.87	2.92	0.00	0.00	10.22	372.26	30.66	1.46
B9	0.00	0.00	0.00	0.00	0.00	0.00	0.00	0.00	269.93	3.19
B10	0.00	0.00	0.00	0.00	0.00	0.00	0.00	0.00	0.00	232.26

Table S5. Connectivity matrix for PLD=50 days and z=1.5 m (in ‰; 2nd period only). Cells in blue colour correspond to self-recruitment values. Cells in brown colour indicate the maximum connectivity value for each box, excluding self-recruitment.

Start\End	B1	B2	B3	B4	B5	B6	B7	B8	B9	B10
B1	646.54	0.00	0.00	0.00	0.00	0.00	0.00	0.00	1.10	0.00
B2	0.00	50.62	94.56	4.78	0.00	0.00	0.00	0.00	56.35	0.00
B3	0.00	6.06	46.71	2.60	0.00	0.00	0.00	0.00	4.33	2.60
B4	0.00	0.00	0.00	60.11	0.00	0.00	0.00	2.12	4.95	0.71
B5	0.00	0.00	0.00	0.00	10.45	0.00	0.00	0.00	3.48	0.00
B6	0.00	0.00	0.00	0.00	0.00	556.84	0.00	0.00	0.00	0.00
B7	0.00	0.00	30.45	3.21	0.00	0.00	650.64	83.33	4.81	3.21
B8	0.00	1.80	1.80	0.00	0.00	0.00	2.69	792.64	3.59	4.49
B9	0.00	1.08	0.00	0.00	0.00	0.00	0.00	4.31	348.44	23.73
B10	0.00	0.00	0.00	0.00	0.00	0.00	0.00	0.00	0.00	271.94

Table S6. Connectivity matrix for PLD=50 days and z=1.5 m (in ‰; 3rd period only). Cells in blue colour correspond to self-recruitment values. Cells in brown colour indicate the maximum connectivity value for each box, excluding self-recruitment.

Start\End	B1	B2	B3	B4	B5	B6	B7	B8	B9	B10
B1	764.32	0.00	0.00	1.08	0.00	0.00	0.00	1.08	1.08	0.00
B2	0.00	25.34	21.44	20.47	0.00	0.00	0.00	0.00	31.19	4.87
B3	0.00	0.00	33.91	11.30	0.00	0.00	0.00	0.00	0.00	12.17
B4	0.00	0.00	0.00	18.88	0.00	0.00	0.00	0.00	116.19	10.89
B5	0.00	0.00	0.00	0.00	73.29	0.00	0.00	0.00	21.17	9.77
B6	0.00	6.70	5.59	2.23	0.00	440.22	93.85	34.64	10.06	1.12
B7	0.00	6.44	3.22	3.22	0.00	0.00	363.93	43.48	30.60	19.32
B8	0.00	2.03	2.03	2.03	2.03	0.00	11.19	263.48	156.66	3.05
B9	0.00	0.00	0.00	0.00	0.00	0.00	0.00	0.00	438.50	11.76
B10	0.00	0.00	0.00	0.00	0.96	0.00	0.00	0.00	0.00	269.75

Table S7. Connectivity matrix for PLD=50 days and z=1.5 m (in ‰; 4th period only). Cells in blue colour correspond to self-recruitment values. Cells in brown colour indicate the maximum connectivity value for each box, excluding self-recruitment.

Start\End	B1	B2	B3	B4	B5	B6	B7	B8	B9	B10
B1	306.30	2.13	13.87	3.20	0.00	0.00	9.61	2.13	0.00	28.82
B2	0.00	278.91	16.52	5.83	0.00	0.00	4.86	0.00	1.94	18.46
B3	0.00	41.40	34.04	5.52	21.16	0.00	0.92	0.00	0.00	15.64
B4	0.00	0.00	0.00	65.25	37.95	0.00	0.00	0.00	0.00	9.99
B5	0.00	0.00	0.00	0.00	36.28	0.00	0.00	0.00	0.00	0.00
B6	0.00	0.00	1.03	1.03	0.00	279.67	12.38	19.61	2.06	5.16
B7	0.00	6.24	7.49	3.75	0.00	0.00	265.92	52.43	21.22	29.96
B8	0.00	1.30	2.61	6.51	0.00	0.00	20.85	354.40	63.84	33.88
B9	0.00	2.13	12.79	14.93	0.00	0.00	0.00	6.40	119.40	42.64
B10	0.00	0.00	0.00	0.00	0.00	0.00	0.00	0.00	0.00	372.02

Table S8. Connectivity matrix for PLD=50 days and z=12 m (in ‰; 1st period only). Cells in blue colour correspond to self-recruitment values. Cells in brown colour indicate the maximum connectivity value for each box, excluding self-recruitment.

Start\End	B1	B2	B3	B4	B5	B6	B7	B8	B9	B10
B1	425.05	3.21	9.64	3.21	0.00	0.00	10.71	7.49	16.06	8.57
B2	0.00	157.13	2.91	5.82	0.00	0.00	3.88	4.85	14.55	2.91
B3	0.00	2.63	31.55	7.01	0.00	0.00	1.75	3.51	7.89	11.39
B4	0.00	0.00	1.31	99.54	7.20	0.00	0.00	0.00	1.96	6.55
B5	0.00	0.00	0.00	9.39	78.25	0.00	0.00	0.00	0.00	3.13
B6	0.00	1.06	1.06	2.13	0.00	155.32	62.77	9.57	2.13	1.06
B7	0.00	6.35	5.08	7.62	0.00	0.00	137.23	67.34	64.80	33.04
B8	0.00	9.38	5.00	10.01	0.00	0.00	10.01	164.48	92.56	42.53
B9	0.00	5.48	18.62	13.14	0.00	0.00	14.24	24.10	148.96	27.38
B10	0.00	0.00	0.00	0.00	0.00	0.00	0.00	0.00	0.97	323.64

Table S9. Connectivity matrix for PLD=50 days and z=25 m (in ‰; 1st period only). Cells in blue colour correspond to self-recruitment values. Cells in brown colour indicate the maximum connectivity value for each box, excluding self-recruitment.